5th International Conference on Experimental Fluid Mechanics ICEFM 2018 Munich
Munich, Germany, July 2-4, 2018

Adaptive drag reduction using a new passive device

Seokbong Chae[1], Seungcheol Lee[1], Jooha Kim[1*], Jae Hwa Lee[1]

[1] Ulsan National Institute of Science and Technology, Department of Mechanical Engineering, Ulsan, Korea

[*] kimjooha@unist.ac.kr

Abstract

In the present study, the drag on a sphere is optimally reduced in a wide range of Reynolds numbers by using a new passive control device. This device is called an adaptive moving ring (AMR) because its size can be adaptively changed according to the wind speed (i.e. Reynolds number). The drag coefficient of the sphere with AMR is empirically modeled as a function of the size of AMR and the Reynolds number to predict how the optimal size of AMR should vary with the Reynolds number. The AMR, when properly tuned, changes its size following the predicted optimal one. The amount of drag reduction compared to smooth sphere monotonically increases with the Reynolds number by up to 74%.

1 Introduction

There have been various passive flow control methods for reducing drag on bluff bodies such as a sphere and a cylinder. Examples of the control device include dimples (Bearman and Harvey, 1976; Choi et al., 2006), surface roughness (Achenbach, 1974) and surface trip wire (Maxworthy, 1969; Son et al., 2011). The detailed mechanisms of drag reduction by the devices are different from each other, but they commonly produce the disturbances for the transition to turbulence for delaying the main separation (Choi et al., 2008). Interestingly, the size of device (e.g. dimple depth, roughness height or trip wire diameter) affects the critical Reynolds number at which the rapid decrease in drag coefficient (so called 'drag crisis') occurs and the amount of drag reduction. That is, as the device size increases, the drag coefficient starts to decrease at a lower critical Reynolds number but the amount of drag reduction also decreases. Therefore, in order to achieve the maximum drag reduction for varying Reynolds numbers, the device size is required to be changed with the Reynolds number. For a conventional control device, however, the device size is fixed regardless of the Reynolds number, and thus the maximum drag reduction can be achieved in a very narrow range of Reynolds numbers. In this study, we introduce a ring-shaped device whose size passively (i.e. without the energy input) varies with the free-stream velocity (i.e. the Reynolds number) for reducing the drag force on a sphere in a wide range of Reynolds numbers. We call this device as AMR (adaptive moving ring) hereafter. The objectives of the present study are (i) to develop a predictive model of the relationship between the optimal size of AMR and the Reynolds number for the maximum drag reduction, and (ii) to validate the drag reduction by AMR through the wind-tunnel experiment.

2 Control device and experimental set-up

2.1 Control device

Figure 1(a) shows the schematic diagram of the sphere model with AMR. The AMR is attached to the linear ball bearing such that it can be moved in the streamwise direction. The tip of AMR, protruded from the sphere surface by l (see the inset), is located at 50° from the stagnation point to generate the disturbance before the main separation occurs. The movement of AMR is controlled by the force balance between the pneumatic pressure on the upstream side of AMR and the spring elastic force on the downstream side of AMR. That is, the protruded length l (i.e. the size of AMR) decreases with increasing the free-stream velocity (i.e. Reynolds number), and vice versa.

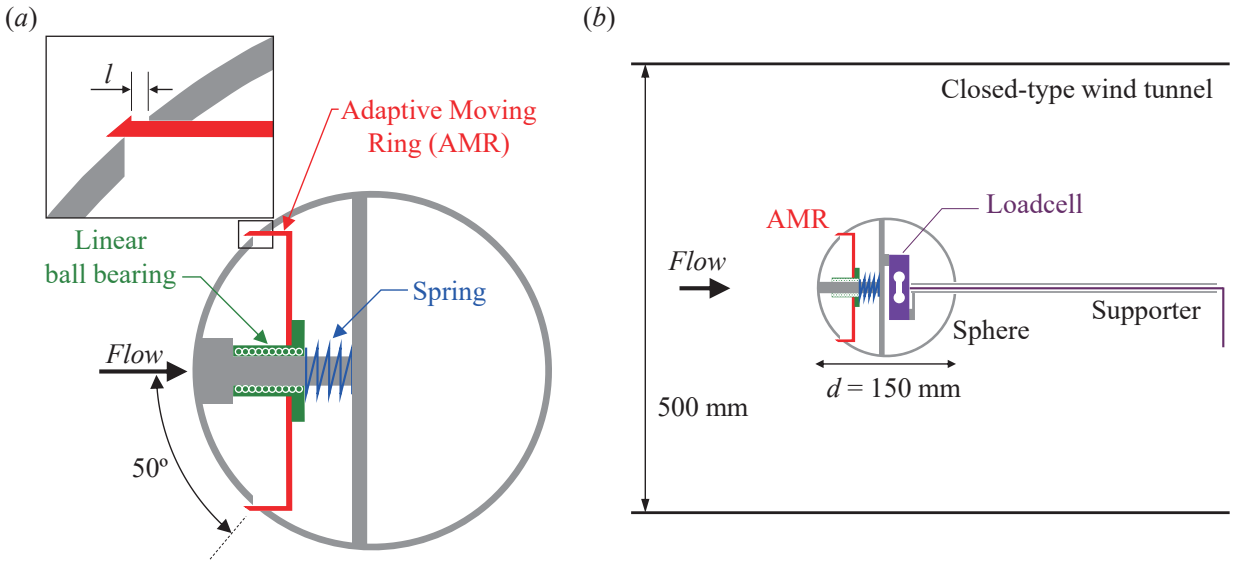

Figure 1: Schematic diagram of (a) the sphere model with AMR and (b) the experimental set-up for the force measurement.

2.2 Experimental set-up

Figure 1(b) shows the experimental set-up for the force measurement. The drag force is directly measured by the loadcell (CAS BCL-2L) installed inside the sphere model through the wind-tunnel experiment. The sphere model is supported from the rear to minimize the support interference. The blockage ratio based on the size of test section (500 mm $\times$ 500 mm) and the sphere diameter (d = 150 mm) is about 7%, being small enough to neglect the blockage effect (Achenbach, 1974). The Reynolds number range for the force measurement is $Re = Ud/\nu = 0.4 \times 10^5 - 4.4 \times 10^5$, where U is the free-stream velocity and ν is the kinematic viscosity of air. The drag force is measured for two cases: (i) when the size of AMR (l/d) is fixed (called 'fixed' AMR hereafter) regardless of the Reynolds number and (ii) when the size of AMR varies depending on the Reynolds number.

3 Results and discussion

3.1 Drag variation for the fixed AMR

Figure 2(a) shows the variations of the drag coefficient with the Reynolds number for the fixed AMR. For $l/d = 0$, the sphere with AMR is almost perfectly round and thus the present results show good agreement with that of smooth sphere Achenbach (1972), showing the reliability of the measurement. At a given l/d, the drag coefficient rapidly decreases at a modified critical Reynolds number and then remains nearly constant with increasing the Reynolds number. This behavior is similar to those of dimples (Bearman and Harvey, 1976; Choi et al., 2006) and surface trip wire (Son et al., 2011). As l/d increases, the drag crisis occurs at lower critical Reynolds number but the minimum drag coefficient increases. Therefore, the optimal size of AMR for maximizing the drag reduction decreases with increasing Reynolds numbers.

3.2 Predictive model for the optimal size of AMR

To find the relationship between the optimal size of AMR and the Reynolds number, we suggest the following empirical model for the prediction of the drag coefficient with the fixed AMR by adopting the parameterized logistic function (Kuss et al., 2005):

$$C_D = C_{D,sub} - |\Delta C_D| \left(1 + \exp\left[\frac{-2\ln 9}{w}(Re - Re_c)\right]\right)^{-1}. \quad (1)$$

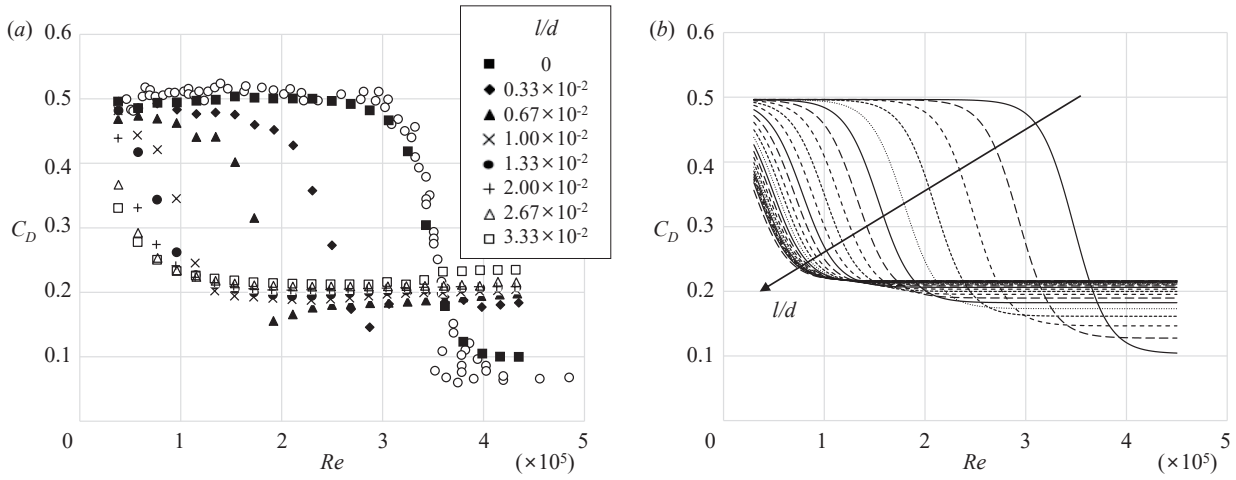

Figure 2: Variations of (*a*) the measured drag coefficient and (*b*) the predicted drag coefficient with the Reynolds number for the fixed AMR. In (*a*) the drag coefficient of a smooth sphere (○; Achenbach, 1972) is also shown for the comparison, and in (*b*) the drag coefficients are shown for $l/d = 0 - 3.33 \times 10^{-2}$ with the interval of 1.33×10^{-3}.

Here $C_{D,sub}$ is the drag coefficient for the Reynolds number smaller than the modified critical Reynolds number, $|\Delta C_D|$ is the amount of drag reduction, w is the width of the Reynolds number range where the drag crisis occurs (i.e. critical Reynolds number range) and Re_c is the central Reynolds number of the critical Reynolds number range. $C_{D,sub}$ can be assumed to be constant regardless of the size of AMR because the drag coefficient converges to almost the same value as the Reynolds number decreases (figure 2*a*). By fitting the drag coefficient with (1) for various l/ds, the relationship between each of the remaining parameters and the size of AMR can be obtained as follows:

$$|\Delta C_D| = 0.11 \exp(-180 l/d) + 0.28, \tag{2}$$

$$w = 74016, \tag{3}$$

$$Re_c = 317200 \exp(-141 l/d) + 29960. \tag{4}$$

It is interesting to note that, as shown in (3), the critical Reynolds number range is nearly constant irrespective of the size of AMR. By combining (1)−(4) the drag coefficient for the fixed AMR can be predicted as shown in figure 2(*b*). The fit of the predicted drag coefficients to the measured ones are very good with r-squared values of 0.91−0.99, where r is the correlation coefficient. Based on the predicted drag coefficient, the optimal size of AMR can be modeled as a function of the Reynolds number using the following logarithmic equation:

$$(l/d)_{opt} = -0.0063 \ln \frac{Re - Re_i}{Re_f - Re_i}. \tag{5}$$

Here Re_i and Re_f denote the modified critical Reynolds numbers for asymptotically high l/d and $l/d = 0$, respectively. Note that the above model is valid for $Re_i < Re < Re_f$ and the detailed derivation is omitted for the sake of brevity.

3.3 Drag variation for AMR

Figure 3 shows the variations of the drag coefficient with the Reynolds number for smooth, dimpled and roughened spheres together with the sphere with AMR. Here, the spring constant is tuned as $\kappa = 720$ N m^{-1} such that the size of AMR can be changed following $(l/d)_{opt}$ in (5). Dimples reduces the drag on a sphere as

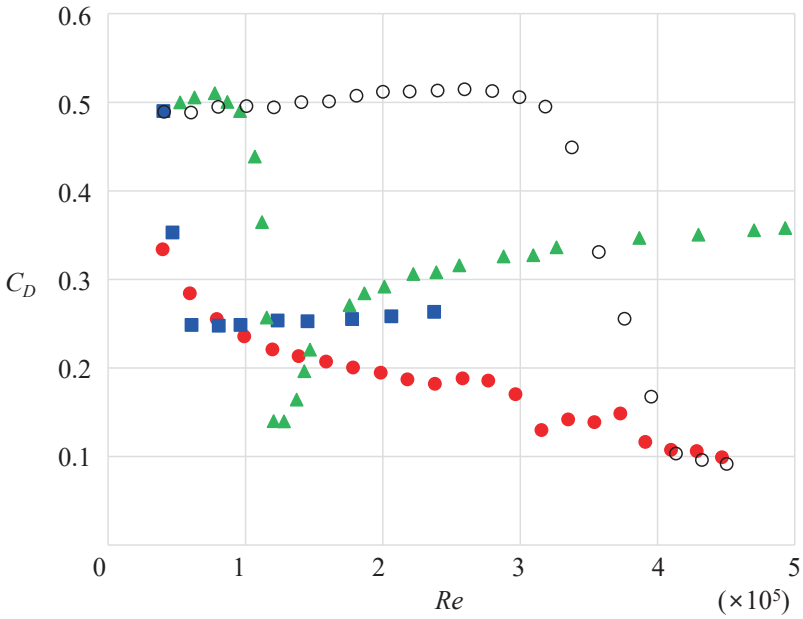

Figure 3: Variations of the drag coefficient with the Reynolds number for smooth, dimpled and roughened spheres together with the sphere with AMR: ○, smooth (present); ■, dimpled ($k/d = 0.9 \times 10^{-2}$, Bearman and Harvey, 1976); ▲, roughened ($k/d = 0.5 \times 10^{-2}$, Achenbach, 1974); ●, AMR (present). Here, k is the depth of dimples or height of roughness.

much as 50%, but the reduced drag coefficient remains nearly constant after the modified critical Reynolds number. Surface roughness also reduces the drag, but the drag coefficient rather increases after the drag crisis occurs. On the other hand, the drag coefficient of the sphere with AMR continuously decreases with the Reynolds number, approaching $C_D \approx 0.1$.

4 Conclusion

Compared with the conventional passive devices, as described above, the most distinguished advantage of the AMR is that the maximum drag reduction can be achieved in a wide range of Reynolds numbers. The drag reduction of a bluff body under varying wind (or water) speed is a very important engineering problem. For example, more than 30% of the total fuel is consumed during take-off and landing for an aircraft on short flights (Romano et al., 1999). Therefore, the AMR can be a potential candidate for efficient and effective adaptive-passive drag reduction.

Acknowledgements

This research was supported by Basic Science Research Program through the National Research Foundation of Korea (NRF) funded by the Ministry of Education (NRF-2016R1D1A1B03933176), and the 2018 Research Fund (1.180015.01) of UNIST (Ulsan National Institute of Science and Technology).

References

Achenbach E (1972) Experiments on the flow past spheres at very high Reynolds numbers. *Journal of Fluid Mechanics* 54:565–575

Achenbach E (1974) The effects of surface roughness and tunnel blockage on the flow past spheres. *Journal of Fluid Mechanics* 65:113–125

Bearman PW and Harvey JK (1976) Golf ball aerodynamics. *Aeronautical Quarterly* 27:112–122

Choi H, Jeon WP, and Kim J (2008) Control of flow over a bluff body. *Annual Review of Fluid Mechanics* 40:113–139

Choi J, Jeon WP, and Choi H (2006) Mechanism of drag reduction by dimples on a sphere. *Physics of Fluids* 18:041702

Kuss M, Jäkel F, and Wichmann FA (2005) Bayesian inference for psychometric functions. *Journal of Vision* 5:478–492

Maxworthy T (1969) Experiments on the flow around a sphere at high Reynolds numbers. *Journal of Applied Mechanics* 36:598–607

Romano D, Gaudioso D, and De Lauretis R (1999) Aircraft emissions: a comparison of methodologies based on different data availability. *Environmental Monitoring and Assessment* 56:51–74

Son K, Choi J, Jeon WP, and Choi H (2011) Mechanism of drag reduction by a surface trip wire on a sphere. *Journal of Fluid Mechanics* 672:411–427